Appendix A

The transformation rate equation essentially comprises two competing "waves". The first wave's kinetics can be described by:

$$f_{\mathrm{UB}}\frac{\mathrm{d}X(T)_{\mathrm{UB}}}{\mathrm{d}T}=f_{\mathrm{UB}}[1-X(T)_{\mathrm{UB}}]\frac{K_{\mathrm{UB}}}{r^2}\int_{T_{s,\mathrm{UB}}}^{T}\exp\left(-\frac{Q_N}{RT}\right)\mathrm{d}T_{\varphi} \tag{A1}$$

where $1-X(T)_{\mathrm{UB}}$ is an increasing function while $\int_{T_{s,\mathrm{UB}}}^{T}\exp\left(-\frac{Q_N}{RT}\right)\mathrm{d}T_{\varphi}$ is decreasing, creating an extremum point. Setting the derivative of Equation (A1) to zero yields:

$$\exp\left(-\frac{Q_N}{RT}\right)-\frac{K_{\mathrm{UB}}}{r^2}\left[\int_{T_{s,\mathrm{UB}}}^{T}\exp\left(-\frac{Q_N}{RT}\right)\mathrm{d}T_{\varphi}\right]^2=0 \tag{A2}$$

The solution to Equation (A2) gives the temperature coordinate $T_{p,\mathrm{UB}}$ of the extremum point. When $T_{s,\mathrm{UB}}$, Q_N and r are given, $T_{p,\mathrm{UB}}$ depends solely on K_{UB}. Thus, knowing both $T_{s,\mathrm{UB}}$ and $T_{p,\mathrm{UB}}$ from the transformation rate curve allows determination of K_{UB}. Furthermore, since the area under the first wave equals f_{UB}, the vertical coordinate of the extremum point is also influenced by f_{UB}.

All transformation rate curves in our study exhibited the characteristics shown in Figure A1, enabling clear identification of $T_{s,\mathrm{UB}}$ and the extremum point for UB transformation. Therefore, the complete fitting procedure is implemented as follows:

i) UB phase fitting: The horizontal coordinate (temperature) of the extremum point in the UB transformation rate curve is used to determine K_{UB}. The vertical coordinate of the extremum point is then employed to further fit f_{UB}. This yields the complete UB transformation rate curve.

ii) LB phase fitting: The LB transformation rate curve is obtained by subtracting the UB contribution from the total transformation rate curve. From this residual curve, both $T_{s,\mathrm{LB}}$ and the extremum point for LB transformation are identified. The temperature coordinate of LB's extremum point is used to determine K_{LB}. Fine-tuning of the parameters is performed to achieve optimal matching between the vertical coordinate of LB's extremum point and the phase volume fraction f_{LB}, where $f_{\mathrm{LB}}=1-f_{\mathrm{UB}}$.

Actually, the fitted values of K_{UB} and K_{LB} were found to be remarkably close, to the extent that using a single value for both parameters could yield equally satisfactory fitting results (this may due to the similar transformation phenomena between UB and LB, particularly continuous nucleation and one-dimensional growth, and the large overlap in their transformation temperature ranges, leading to comparable kinetic behaviors). This result is consistent with our previous findings [13].

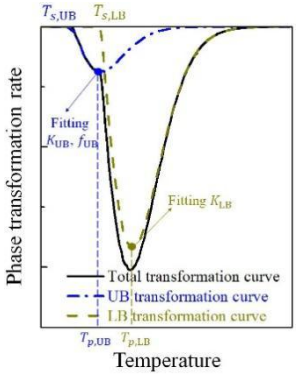

Figure A1 The exhibited general characteristics of the phase transformation curves in the present work: The extremum point of the first wave can be confirmed

Appendix B

The fundamental proportionality $N \propto {L_{\geq x}}^3$ is derived through the following logical progression (where, N_{2D} represents the areal density of bainite packets (number per unit area), d_p denotes the cross-sectional bainite packet size, $\overline{d_p}$ indicates the average packet size, and L corresponds to the total grain boundary length per unit area):

Firstly, assume that bainite packets are approximately circular. The grain size generally follows a log-normal distribution $p(d_p, w, \mu) = \frac{1}{w d_p \sqrt{2\pi}} e^{\frac{(\ln d_p - \mu)^2}{2w^2}}$. Thus, Relationship between N_{2D}, d_p, and L can be given as:

$$N_{2D} \int_0^\infty p(d_p, w, \mu) \pi d_p \mathrm{d}d_p = 2L \tag{A3a}$$

Through variable substitution ($y = \ln d_p$, $z = \frac{y - w^2 - \mu}{\sqrt{2}w}$ and $z' = \frac{y - 2w^2 - \mu}{\sqrt{2}w}$), we derive:

$$\int_0^\infty p(d_p, w, \mu) d_p \mathrm{d}d_p = \frac{1}{w\sqrt{2\pi}} \int_{-\infty}^\infty e^{-\frac{(y-\mu)^2 - 2w^2 y}{2w^2}} \mathrm{d}y = \frac{1}{w\sqrt{2\pi}} e^{-\frac{\mu^2 - \left(w^2 + \mu\right)^2}{2w^2}} \int_{-\infty}^\infty \sqrt{2} w e^{-z^2} \mathrm{d}z =$$

$$e^{\mu + w^2/2} = \overline{d_p} \tag{A3b}$$

Yielding:

$$N_{2D} \overline{d_p} \pi = 2L \tag{A3c}$$

Relationship between the nucleation number per unit volume N and N_{2D} can be given as [36,37]

$$N = N_{2D} / \overline{d_p} \tag{A4}$$

The mean grain size in cross section inverses with the total grain boundary length (based on our previous work, for equiaxed grains or non-equiaxed grains [35]), which gives:

$$\overline{d_p} \cong \frac{1}{L} \tag{A5}$$

Combining (A3c), (A4), and (A5):

$$N \cong \frac{2}{\pi} L^3 \tag{A6}$$

Secondly, recognizing that bainite packets deviate from circularity, we introduce a shape factor β (similar coefficients have been used in establishing relationships for N and N_{2D} of non-equiaxed grains [37,38]):

$$N \cong \beta L^3 \tag{A7}$$

Hence, the approximation $\boldsymbol{N \propto L^3}$ holds. Since bainite packet boundaries are predominantly high-angle grain boundaries, using $L_{\geq x}$ (instead of L) is more physically meaningful. This leads to our final expression Equation (11a).

Appendix C

This relationship in Figure 12(f) can also be validated through EBSD-based analysis using the following methodology:

(i) Utilizing the fact that bainite packet boundaries correspond to high-angle grain boundaries, we first determine N_{2D} from orientation imaging microscopy (OIM) maps generated by EBSD analysis.

(ii) The three-dimensional density parameter N is then computed from the obtained N_{2D} values.

(iii) Applying Equation (10), we estimate N_0 values for comparative analysis.

Using Image-Pro Plus software, the number of bainite packets ($n^{'}$) in the scanned area (A_{scan}) was measured [35] (to avoid miscounting or misidentifying very small bainite packets, those with an area smaller than 4 pixels were uniformly excluded during measurement):

$$n^{'} = n^{'}_{\mathrm{inside}} + \frac{n^{'}_{\mathrm{intercepted}}}{2} \tag{A8}$$

where, $n^{'}_{\mathrm{inside}}$ is the number of grains completely within the field view and $n^{'}_{\mathrm{intercepted}}$ is the number of grains intercepted by the edges of the field view. Thus, N_{2D} can be calculated as:

$$N_{2D} \cong \frac{n^{'}}{A_{\mathrm{scan}}} \tag{A9}$$

To calculate the average packet size $\overline{d_{\mathrm{p}}}$, the following equation can be used [35] (though an alternative form $\overline{d_{\mathrm{p}}} \cong \frac{1}{L_{\geq 15}}$ from Equation (A5) could also be employed, as the resulting trend of N_0 value remains consistent):

$$\overline{d_{\mathrm{p}}} \cong \sqrt{\frac{4A_{\mathrm{scan}}}{\pi n^{'}}} \tag{A10}$$

Using Equation (A4), we then obtain:

$$N = \left(\frac{n^{'}}{A_{\mathrm{scan}}}\right)^{3/2} \sqrt{\frac{\pi}{4}} \tag{A11}$$

Then, using the mathematical relationship in Equation (10), we obtain:

$$N_0 \cong \left(\frac{n^{'}}{A_{\mathrm{scan}}}\right)^{3/2} \sqrt{\frac{\pi}{4}} \cdot r / \int_{T_{f,\mathrm{LB}}}^{T_{s,\mathrm{LB}}} \exp\left(-\frac{Q_N}{RT}\right) \mathrm{d}T \tag{A12}$$

We calculated N_0 for specimens 1623-50-7, 1623-50-10, 1623-50-14, 1373-50-7, 1373-50-10, and 1373-50-14, with the results listed in Table A1. These results further support the conclusion that N_0 increases with cooling rate, but the rate of increase trends to diminish (or remain comparable) as r becomes larger.

Table A1 N_0 values calculated through EBSD-derived bainite packet statistics

Sample	Volumetric PAGS/μm	EBSD step size/μm	$n^{'}$	N_{2D}/m^{-2}	N/m^{-3}	$N_0/(\mathrm{m}^{-3}\cdot \mathrm{s}^{-1})$
1623-50-7	138.6	2.5	260	1.0E+9	2.9E+13	1.3E+17
1623-50-10			238	9.4E+8	2.6E+13	2.4E+17
1623-50-14			208.5	8.2E+8	2.1E+13	4.1E+17

1373-50-7	21.1	0.5	138	1.4E+10	1.4E+15	4.7E+18
1373-50-10			178	1.8E+10	2.1E+15	1.3E+19
1373-50-14			116	1.1E+10	1.1E+15	1.7E+19

It should be emphasized that certain small bainite packets— particularly those with dimensions below the EBSD step size threshold— were systematically excluded from statistical evaluation. As the relative abundance of these sub-resolution packets varies substantially with different EBSD step sizes, the derived n' values may demonstrate some variation. This inherent variability consequently renders N_{2D} measurements acquired at differing step sizes non-comparable, potentially introducing inconsistencies in subsequent N_0 calculations. Nevertheless, since undersized packets typically represent only a marginal proportion of the total population, their influence on cumulative boundary length measurements remains insignificant. The negligible contribution of these omitted small packets to the total boundary length ensures analytical robustness, as their exclusion introduces minimal distortion in quantitative assessments. This fundamental characteristic establishes grain boundary length analysis as intrinsically more dependable than direct packet counting approaches when comparing datasets obtained with varying EBSD step sizes.